

Decomposition of Uncertainty for Active Learning and Reliable Reinforcement Learning in Stochastic Systems

Stefan Depeweg
Siemens AG, TU Munich

José Miguel Hernández-Lobato
University of Cambridge

Finale Doshi-Velez
Harvard University

Steffen Udluft
Siemens AG

Abstract

Bayesian neural networks (BNNs) with latent variables are probabilistic models which can automatically identify complex stochastic patterns in the data. We study in these models a decomposition of predictive uncertainty into its epistemic and aleatoric components. We show how such a decomposition arises naturally in a Bayesian active learning scenario and develop a new objective for reliable reinforcement learning (RL) with an epistemic and aleatoric risk element. Our experiments illustrate the usefulness of the resulting decomposition in active learning and reliable RL.

1 Introduction

Many important problems require learning stochastic functions. For example, in reinforcement learning, the transition dynamics of a system are often stochastic. Recent advances in training Bayesian neural network (BNN) models have greatly enhanced the applicability of these models to the point that they have become the go-to function approximator in many reinforcement learning settings (e.g. [Gal et al., 2016, Blundell et al., 2015, Houthoofd et al., 2016]). In particular, recent work has extended BNNs with a latent variable model to describe complex stochastic functions [Depeweg et al., 2016, Moerland et al., 2017]. Here, the BNNs encode a probability distribution over stochastic functions of a continuous Markov Decision Process (MDP). This probability distribution can then be used for policy search, by finding the optimal policy with respect to state trajectories simulated from the model. The BNNs with latent variables produce improved probabilistic predictions and these result in better performing policies.

That said, learning an unknown stochastic function, especially from limited data, can be challenging because there

are two sources of uncertainty: one from a lack of knowledge about the stochastic function, and one from the inherent stochasticity of the function itself. Kiureghian and Ditlevsen [2009] name these *epistemic* and *aleatoric* uncertainties, respectively. This distinction is important because these uncertainties are fundamentally different in nature: in the Bayesian setting, epistemic uncertainty is closely tied to our subjective probabilities over models; it is the source of model (or representational) bias (see e.g. Joseph et al. [2013]). An error in estimating the ground truth MDP at even a single transition step can render the complete policy useless (see e.g. Schneegass et al. [2008]). In contrast, aleatoric uncertainty is the source of inherent variance.

In this work, we first derive the decomposition of the uncertainty present in the predictions of BNNs with latent variables into its epistemic and aleatoric components. We derive two ways of quantifying these uncertainties: through their (conditional) entropies and through their variances. Next we demonstrate the usefulness of such decompositions in two different domains: active learning and reliable reinforcement learning. To our knowledge, ours is the first work to provide an active learning scheme for arbitrarily complex stochastic functions. Finally, we use our decomposition to develop a novel criterion for reliable reinforcement learning. We demonstrate that our approach allows a domain expert to trade-off the risks of model bias and domain stochasticity, and also that different real-world domains require different trade-offs for good performance.

2 Background: Bayesian Neural Networks with Latent Variables

Bayesian Neural Networks (BNNs) are scalable and flexible probabilistic models. In this work, we use this class of models as the basic building block, so in the following we want to start to give a brief summary of the key concepts.

Given data $\mathcal{D} = \{\mathbf{x}_n, \mathbf{y}_n\}_{n=1}^N$, formed by feature vectors $\mathbf{x}_n \in \mathbb{R}^D$ and targets $\mathbf{y}_n \in \mathbb{R}^K$, we assume that $\mathbf{y}_n = f(\mathbf{x}_n, z_n; \mathcal{W}) + \epsilon_n$, where $f(\cdot, \cdot; \mathcal{W})$ is the output of a neural network with weights \mathcal{W} and K output units. The network receives as input the feature vector \mathbf{x}_n and the latent variable $z_n \sim \mathcal{N}(0, \gamma)$. We choose

rectifiers: $\varphi(x) = \max(x, 0)$ as activation functions for the hidden layers and the identity function: $\varphi(x) = x$ for the output layer. The network output is corrupted by the additive noise variable $\epsilon_n \sim \mathcal{N}(\mathbf{0}, \Sigma)$ with diagonal covariance matrix Σ . The role of the latent variable z_n is to capture unobserved stochastic features that can affect the network's output in complex ways. Without z_n , randomness would only be given by the additive Gaussian observation noise ϵ_n , which can only describe limited stochastic patterns. The network has L layers, with V_l hidden units in layer l , and $\mathcal{W} = \{\mathbf{W}_l\}_{l=1}^L$ is the collection of $V_l \times (V_{l-1} + 1)$ weight matrices. The $+1$ is introduced here to account for the additional per-layer biases. We approximate the exact posterior distribution $p(\mathcal{W}, \mathbf{z} | \mathcal{D})$ with:

$$q(\mathcal{W}, \mathbf{z}) = \underbrace{\prod_{l=1}^L \prod_{i=1}^{V_l} \prod_{j=1}^{V_{l-1}+1} \mathcal{N}(w_{ij,l} | m_{ij,l}^w, v_{ij,l}^w)}_{q(\mathcal{W})} \times \underbrace{\left[\prod_{n=1}^N \mathcal{N}(z_n | m_n^z, v_n^z) \right]}_{q(\mathbf{z})}. \quad (1)$$

The parameters $m_{ij,l}^w, v_{ij,l}^w$ and m_n^z, v_n^z are determined by minimizing a divergence between $p(\mathcal{W}, \mathbf{z} | \mathcal{D})$ and the approximation q . For more detail the reader is referred to the work of Hernández-Lobato et al. [2016], Depeweg et al. [2016]. In our experiments we use black-box α -divergence minimization with $\alpha = 1.0$, for the experiment to follow we observed that this provided the best decomposition of uncertainty. In the supplementary material we show results obtained using $\alpha = 0.5$ and variational Bayes ($\alpha = 0$).

3 Main Idea: Uncertainty Decomposition in BNNs with Latent Variables

BNNs with latent variables can describe complex stochastic patterns while at the same time account for model uncertainty. They achieve this by jointly learning $q(\mathbf{z})$, which captures the specific values of the latent variables in the training data, and $q(\mathcal{W})$, which represents any uncertainty about the model parameters. The result is a principled Bayesian approach for learning flexible stochastic functions.

For these models, we can identify two types of uncertainty: *aleatoric* and *epistemic* [Kiureghian and Ditlevsen, 2009, Kendall and Gal, 2017]. Aleatoric uncertainty originates from random latent variables, whose randomness cannot be reduced by collecting more data. In the BNNs this is given by $q(\mathbf{z})$ and the additive Gaussian noise ϵ . Epistemic uncertainty, on the other hand, originates from lack of statistical evidence and can be reduced by gathering more data. In the BNN this is given by $q(\mathcal{W})$, which captures uncertainty over the model parameters.

These two forms of uncertainty are entangled in the approximate predictive distribution:

$$p(y_* | \mathbf{x}_*) = \int p(y_* | \mathcal{W}, \mathbf{x}_*, z) p(z_*) q(\mathcal{W}) dz_* d\mathcal{W}. \quad (2)$$

where $p(y_* | \mathcal{W}, \mathbf{x}_*, z_*) = \mathcal{N}(y_* | f(\mathbf{x}_*, z_*; \mathcal{W}), \Sigma)$ is the likelihood function of the BNN and $p(z_*) = \mathcal{N}(z_* | 0, \gamma)$ is the prior on the latent variables. If, instead of integrating with respect to \mathcal{W} , we keep it fixed to a particular value \mathbf{w} , we obtain a predictive distribution $p(y_* | \mathbf{x}_*, \mathcal{W} = \mathbf{w})$ with only aleatoric uncertainty. By integrating then with respect to $q(\mathcal{W})$, we obtain a distribution with both epistemic and aleatoric uncertainty. In this work, we disentangle the two forms of uncertainty present in (2) and illustrate the usefulness of the resulting decomposition in active learning and reliable RL settings. Below we describe two decompositions, each quantifying uncertainty in a different way.

The first metric is the entropy, given by $H[p(X)] = \mathbb{E}_{p(X)}[-\log p(X)]$ for the random variable X with probability distribution $p(X)$. To perform our uncertainty decomposition, we also make use of the conditional entropy, given by $H[Y|X] = \mathbb{E}_{p(X=x)} H[p(Y|X=x)]$ for the two random variables X and Y . The total uncertainty present in (2) can be measured by the entropy of this distribution, that is, $H[p(y_* | \mathbf{x}_*)]$. In the BNN predictive distribution, the entropy of y_* given \mathbf{x}_* when we condition on \mathcal{W} is

$$H[y_* | \mathcal{W}, \mathbf{x}_*] = \mathbb{E}_{q(\mathcal{W})} \left[H \left(\int p(y_* | \mathcal{W}, \mathbf{x}_*, z_*) p(z_*) dz_* \right) \right].$$

The entropy inside of the expectation in this expression quantifies the uncertainty originated by the latent variable z_* and the additive Gaussian noise $\epsilon \sim \mathcal{N}(0, \Sigma)$. Therefore, this expression measures the *aleatoric* uncertainty present in (2). By calculating $H[p(y_* | \mathbf{x}_*)] - H[y_* | \mathcal{W}, \mathbf{x}_*]$ we obtain the uncertainty in the random variable y_* that is not aleatoric. This is the *epistemic* uncertainty of y_* .

Instead of the entropy, we can also use the variance $\sigma^2(y_* | \mathbf{x}_*)$ as a measure of uncertainty. In this case, a decomposition is straightforward using the law of total variance:

$$\sigma^2(y_* | \mathbf{x}_*) = \sigma_{q(\mathcal{W})}^2(\mathbb{E}[y_* | \mathcal{W}, \mathbf{x}_*]) + \mathbb{E}_{q(\mathcal{W})}[\sigma^2(y_* | \mathcal{W}, \mathbf{x}_*)].$$

We see that the variance is composed of two terms. The first one, $\sigma_{\mathcal{W}}^2(\mathbb{E}[y_* | \mathcal{W}], \mathbf{x}_*)$ is the variability of y_* , when we integrate out z_* but not \mathcal{W} . This is a measure of the *epistemic* uncertainty. The second term, $\mathbb{E}_{\mathcal{W}}[\sigma^2(y_* | \mathcal{W}, \mathbf{x}_*)]$, is similar to the conditional entropy: it represents the average variability of y_* not originating from \mathcal{W} . This measures the *aleatoric* uncertainty. In some applications, working with the variance can be undesirable because it represents variability in square units, instead of in the original units. To avoid this, we can work with the standard deviation:

$$\sigma(y_* | \mathbf{x}_*) = (\sigma_{q(\mathcal{W})}^2(\mathbb{E}[y_* | \mathcal{W}, \mathbf{x}_*]) + \mathbb{E}_{q(\mathcal{W})}[\sigma^2(y_* | \mathcal{W}, \mathbf{x}_*)])^{\frac{1}{2}}.$$

4 Active Learning of Stochastic Functions

Active learning is the problem of iteratively choosing training data so that the resulting gains in predictive performance are as high as possible. Here, we extend the information-theoretic approach based on the expected reduction in entropy of the posterior distribution [MacKay, 1992] for general stochastic functions via a novel Bayesian procedure.

We start by deriving the expected reduction in entropy in BNNs with latent variables. We assume a scenario in which a BNN with latent variables has been fitted to a batch of data $\mathcal{D} = \{(\mathbf{x}_1, \mathbf{y}_1), \dots, (\mathbf{x}_N, \mathbf{y}_N)\}$ to produce a posterior approximation $q(\mathcal{W}, \mathbf{z})$. The expected reduction in posterior entropy for \mathcal{W} when \mathbf{x}_* is incorporated into \mathcal{D} is

$$H(\mathcal{W}|\mathcal{D}) - \mathbb{E}_{y_*|\mathbf{x}_*, \mathcal{D}} \left[H(\mathcal{W}|\mathcal{D} \cup \{\mathbf{x}_*, y_*\}) \right] \quad (3)$$

$$= H(\mathcal{W}) - H(\mathcal{W}|y_*) \quad (4)$$

$$= I(\mathcal{W}; y_*) \quad (5)$$

$$= H(y_*) - H(y_*|\mathcal{W}) \quad (6)$$

$$= H \left[\int_{\mathcal{W}, z_*} p(y_*|\mathcal{W}, \mathbf{x}_*, z_*) q(\mathcal{W}) p(z_*) dz_* d\mathcal{W} \right] - \mathbb{E}_{q(\mathcal{W})} \left[H \left(\int_{z_*} p(y_*|\mathcal{W}, \mathbf{x}_*, z_*) p(z_*) dz_* \right) \right] \quad (7)$$

where $I(\cdot; \cdot)$ denotes the mutual information between two random variables.

In Eq. 7 we see that the epistemic uncertainty we introduced in Section 3 arises naturally in this setting: the most informative points in a stochastic function are those, where the epistemic uncertainty is the highest. The epistemic uncertainty is the difference between the full uncertainty $H(y_*)$ and the aleatoric uncertainty given by $H(y_*|\mathcal{W})$.

The quantity in equation (7) can be approximating using standard entropy estimators, e.g. nearest-neighbor methods [Kozachenko and Leonenko, 1987, Kraskov et al., 2004, Gao et al., 2016]. For that, we repeatedly sample \mathcal{W} and z_* and do forward passes through the neural network to sample y_* . The resulting samples of y_* can then be used to approximate the respective entropies for each \mathbf{x}_* using the nearest-neighbor approach:

$$H(y_*|\mathbf{x}_*, \mathcal{D}) - \mathbb{E}_{q(\mathcal{W})} \left[H \left(\int_{z_*} p(y_*|\mathcal{W}, \mathbf{x}_*, z_*) p(z_*) dz_* \right) \right] \approx \hat{H}(y_1, \dots, y_L) - \frac{1}{M} \sum_{i=1}^M \left[\hat{H}(y_1^{\mathbf{w}_i}, \dots, y_L^{\mathbf{w}_i}) \right]. \quad (8)$$

where $\hat{H}(\cdot)$ computes the nearest-neighbor estimate of the entropy given by an empirical sample of points, $y_1, \dots, y_L \sim p(y_*|\mathbf{x}_*, \mathcal{D})$, $\mathbf{w}_1, \dots, \mathbf{w}_M \sim q(\mathcal{W})$ and $y_1^{\mathbf{w}_i}, \dots, y_L^{\mathbf{w}_i} \sim p(y_*|\mathbf{x}_*, \mathcal{D}, \mathbf{w}_i)$ for $i = 1, \dots, M$.

4.1 Experiments

We now will illustrate the active learning procedure described in the previous section on three examples. In each

problem we will first train a BNN with 2 layers and 20 units in each layer on the available data. Afterwards, we approximate the information-theoretic measures as outlined in the previous section. In the supplementary material we include results using Hamiltonian Monte Carlo, blackbox- α divergence minimization with $\alpha = 0.5$ and VB for the first two toy problems.

Uncertainty decompositions can identify informative inputs in the presence of heteroskedastic noise.

We consider regression for a stochastic function with heteroskedastic noise: $y = 7 \sin(x) + 3|\cos(x/2)|\epsilon$ with $\epsilon \sim \mathcal{N}(0, 1)$. We sample 750 values of the input x from a mixture of three Gaussians with mean parameters $\{\mu_1 = -4, \mu_2 = 0, \mu_3 = 4\}$, variance parameters $\{\sigma_1 = \frac{2}{5}, \sigma_2 = 0.9, \sigma_3 = \frac{2}{5}\}$ and with each Gaussian component having weight equal to $1/3$ in the mixture. Figure 1a shows the raw data. We have many points at the borders and in the center, but little in between.

Figure 1 visualizes the respective quantities. The BNN with latent variables accurately decomposes of its predictive uncertainty between epistemic uncertainty and aleatoric uncertainty: the reduction in entropy approximation, shown in Figure 1f, is inversely proportional to the density used to sample the data (shown in Figure 1b). This makes sense, since in this toy problem the most informative data points are expected to be located in regions where data is scarce. (In more complicated settings, the most informative data points may not satisfy this property.)

Uncertainty decompositions can identify informative inputs in the presence of bimodal stochastic functions.

Next we consider a toy problem given by a regression task with bimodal data. We define $x \in [-0.5, 2]$ and $y = 10 \sin(x) + \epsilon$ with probability 0.5 and $y = 10 \cos(x) + \epsilon$, otherwise, where $\epsilon \sim \mathcal{N}(0, 1)$ and ϵ is independent of x . The data availability is not uniform in x ; we sample 750 values of x from an exponential distribution with $\lambda = 2$

Figure 2 visualizes the respective quantities. The predictive distribution shown in Figure 2c shows the BNN has learned the bimodal structure in the data. The predictive distribution gets increasingly ‘washed out’ as we increase x_* . This increase in entropy as a function of x_* is seen in Figure 2d. The conditional entropy $H(y_*|\mathcal{W})$ of the predictive distribution shown in Figure 2e appears to be symmetric around $x = 0.75$. All this demonstrates the BNN has correctly learned to separate the aleatoric component from the full uncertainty: the ground truth function is symmetric around $x = 0.75$ at which point it changes from a bimodal to a unimodal stochastic function. Figure 2f shows the estimate of reduction in entropy for each x . Here we can observe two effects: First, as expected, the expected entropy reduction increases with higher x . Second, we see a slight decrease from $x = -0.5$ to $x = 0.75$. The reason for this is twofold: because the data is limited to $[-0.5, 2]$, we expect a higher

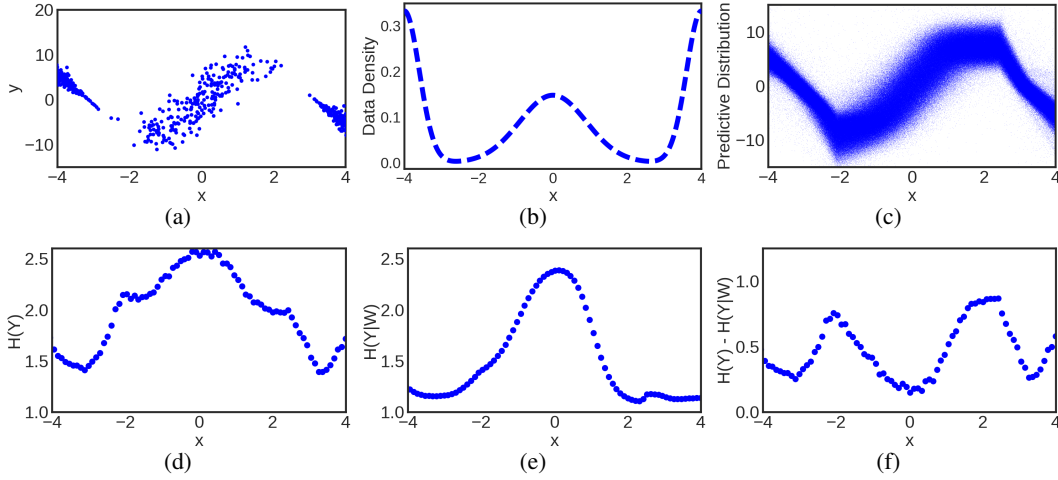


Figure 1: Active learning example using heteroskedastic data. (a): Raw data. (b): Density of x in raw data. (c): Predictive distribution: $p(y_\star|x_\star)$ of BNN. (d): Entropy estimate $H(y_\star|x_\star)$ of predictive distribution for each x_\star . (e): Conditional entropy estimate $\mathbb{E}_{q(\mathcal{W})} H(y_\star|x_\star, \mathcal{W})$. (f): Estimate of reduction in entropy.

level of uncertainty in the vicinity of both borders. Furthermore, learning a bimodal function requires more data to reach the same level of confidence than a unimodal function.

Uncertainty decompositions can identify informative inputs in the presence of heterogeneous stochastic patterns. In our third experiment we consider data generated by a two-dimensional stochastic system, the wetchicken dynamics. For a detailed description we refer to Hans and Udfluft [2009], Depeweg et al. [2016]. The dynamics of this benchmark give rise to complex transition distributions, including bimodality, heteroskedasticity and truncated uniform distributions. We sample 7500 state transitions using random exploration, as shown in Fig. 3a. The reduction in entropy, shown in Fig. 3d is the highest in the bottom right corner. This makes sense, as reaching the bottom is very rare with random exploration – often the agent will already have fallen down the waterfall prior reaching this area.

5 Reliable Reinforcement Learning by Minimizing Model Bias Risk

We now derive a new objective for reliable model-based RL, one that optimizes policy quality (minimizes costs) and policy reliability (when evaluated on the ground truth system policies should not deviate significantly from the performance predicted at training time). Such an approach is important for complex industrial systems and in population settings, e.g. public health: stochasticity may be inevitable as different people will respond differently to interventions. However, before rolling out an expensive program, one would like an accurate forecast of how the intervention will affect the population. Similarly, stochasticity may be, to some extent, inevitable in manufacturing processes, but

before changing the process, one would like an accurate forecast of the new distribution of manufacturing errors.

Similar to Depeweg et al. [2016], we focus on the batch reinforcement learning setting, as this setting is most common in the kind of contexts we described above. In the batch reinforcement learning setting, we are given a batch of state transitions $\mathcal{D} = \{(s_t, \mathbf{a}_t, s_{t+1})\}$ formed by triples containing the current state s_t , the action applied \mathbf{a}_t and the next state s_{t+1} . For example, \mathcal{D} may be formed by measurements taken from an already-running system. In addition to \mathcal{D} , we are also given a cost function c . The goal is to obtain from \mathcal{D} a policy in parametric form that minimizes c on average under the system dynamics. We note that in this setting, the agent’s knowledge about the system dynamics is limited to the available batch; some areas in state space may be over- or underrepresented.

The aforementioned problem can be solved using model-based policy search methods. These methods include two key parts [Deisenroth et al., 2013]. The first part consists in learning a dynamics model from \mathcal{D} . We assume that the true dynamical system can be expressed by an unknown neural network with stochastic inputs:

$$\mathbf{s}_t = f_{\text{true}}(\mathbf{s}_{t-1}, \mathbf{a}_{t-1}, z_t; \mathcal{W}_{\text{true}}), \quad z_t \sim \mathcal{N}(0, \gamma), \quad (9)$$

where $\mathcal{W}_{\text{true}}$ denotes the synaptic weights of the network and \mathbf{s}_{t-1} , \mathbf{a}_{t-1} and z_t are the inputs to the network. In the second part of our model-based policy search algorithm, we optimize a parametric policy given by a deterministic neural network with synaptic weights \mathcal{W}_π . This parametric policy computes the action \mathbf{a}_t as a function of \mathbf{s}_t , that is, $\mathbf{a}_t = \pi(\mathbf{s}_t; \mathcal{W}_\pi)$. We optimize \mathcal{W}_π to minimize the expected cost $C = \sum_{t=1}^T c_t$ over a finite horizon T with respect to our belief $q(\mathcal{W})$, where $c_t = c(\mathbf{s}_t)$. This expected cost is obtained by averaging over multiple virtual roll-outs.

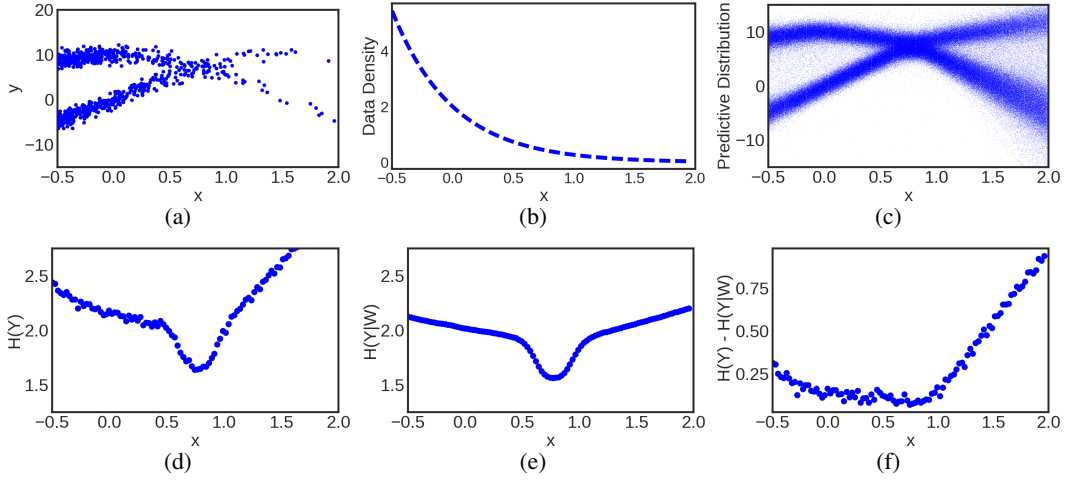


Figure 2: Active learning example using bimodal data. (a): Raw data. (b): Density of x in raw data. (c): Predictive distribution: $p(y_*/x_*)$ of BNN. (d): Entropy estimate $H(y_*/x_*)$ of predictive distribution for each x_* . (e): Conditional entropy estimate $\mathbf{E}_{q(\mathcal{W})} H(y_*/x_*, \mathcal{W})$. (f): Estimate of reduction in entropy.

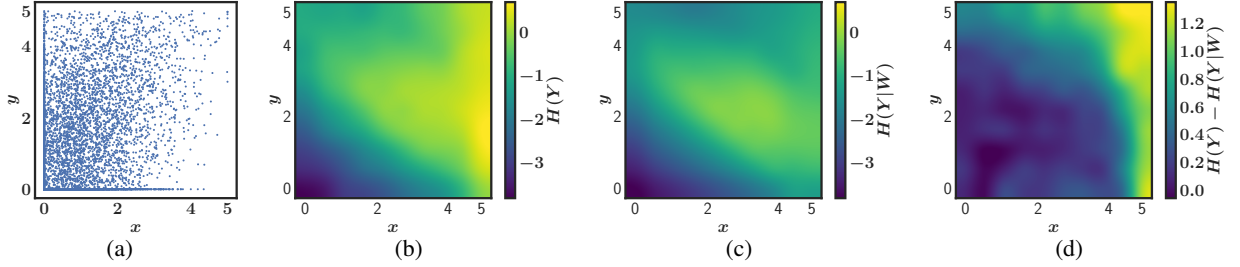


Figure 3: Active learning on wetchicken dynamics. (a): Raw data. (b): Entropy estimate $H(\mathbf{s}_{t+1}|\mathbf{s}_t)$ of predictive distribution for each \mathbf{s}_t (using $\mathbf{a}_t = \{0, 0\}$). (c): Conditional entropy estimate $\mathbf{E}_{q(\mathcal{W})} H(\mathbf{s}_{t+1}|\mathbf{s}_t, \mathcal{W})$. (d): Estimated entropy reduction.

For each roll-out we choose \mathbf{s}_0 randomly from the states in \mathcal{D} , sample $\mathcal{W}_i \sim q$ and then simulate state trajectories using the model $\mathbf{s}_{t+1} = f(\mathbf{s}_t, \mathbf{a}_t, z_t; \mathcal{W}_i) + \epsilon_{t+1}$ with policy $\mathbf{a}_t = \pi(\mathbf{s}_t; \mathcal{W}_\pi)$, input noise $z_t \sim \mathcal{N}(0, \gamma)$ and additive noise $\epsilon_{t+1} \sim \mathcal{N}(\mathbf{0}, \Sigma)$. This procedure allows us to obtain estimates of the policy’s expected cost for any particular cost function. If model, policy and cost function are differentiable, we are then able to tune \mathcal{W}_π by stochastic gradient descent over the roll-out average.

Given the cost function c , the objective to be optimized by the policy search algorithm is

$$J(\mathcal{W}_\pi | \mathbf{s}_0) = \mathbf{E}_{q(\mathcal{W})} [C | \mathbf{s}_0] = \mathbf{E}_{q(\mathcal{W})} \left[\sum_{t=1}^T c_t \right]. \quad (10)$$

Standard approaches in risk-sensitive RL [García and Fernández, 2015] use the standard deviation of the cumulative cost C as risk measure. High risk is associated to high variability in the cost C . The new objective is:

$$J(\mathcal{W}_\pi | \mathbf{s}_0) = \mathbf{E}[C | \mathbf{s}_0] + \beta \sigma(C | \mathbf{s}_0), \quad (11)$$

where $\sigma(C)$ denotes the standard deviation of the cost and the free parameter β determines the amount of risk-avoidance ($\beta \geq 0$) or risk-seeking behavior ($\beta < 0$).

In this work we will focus on risk measures based on individual costs c_t instead of the cumulative cost C , because, as we will see later, this gives us a more strict measure of risk. The variability of the cost $\sigma(c_t)$ originates from two different sources. First, from the existing uncertainty over the model parameters and secondly, from the intrinsic stochasticity of the dynamics. To see this we use the uncertainty decomposition of the variance from Section 3:

$$\sigma(c_t) = (\sigma_{q(\mathcal{W})}^2(\mathbf{E}[c_t | \mathcal{W}]) + \mathbf{E}_{q(\mathcal{W})}[\sigma^2(c_t | \mathcal{W})])^{\frac{1}{2}}. \quad (12)$$

We note that $\mathbf{E}[c_t | \mathcal{W}]$ is the expected cost of a policy \mathcal{W}_π under the dynamics given by \mathcal{W} . The expectation integrates out the influence of the latent variables z_1, \dots, z_t and the output noise $\epsilon_1, \dots, \epsilon_t$.

Next we show that $\sigma_{q(\mathcal{W})}(\mathbf{E}[c_t | \mathcal{W}])$ indeed represents episodic uncertainty of the model by connecting it to the concept of model bias. We use the standard deviation instead of

variance here, because it has the same units as the cost. We define model bias as the discrepancy of policy performance under a) the assumed model and b) the ground truth MDP. While we cannot avoid the existence of such discrepancy when data is limited, we wish to guide the policy search towards policies that stay in state spaces where the risk for model-bias is low. Thus, we define the model bias b as:

$$b(\mathcal{W}_\pi | \mathbf{s}_0) = \sum_{t=1}^T |\mathbf{E}_{\text{true}}[c_t] - \mathbf{E}_{q(\mathcal{W})}[c_t]|, \quad (13)$$

where $\mathbf{E}_{\text{true}}[c_t]$ is the expected cost obtained at time t when starting at the initial state \mathbf{s}_0 and the ground truth dynamics are evolved according to policy $\pi(\mathbf{s}_t; \mathcal{W}_\pi)$. Focusing on individual costs c_t is more strict than comparing the expected cumulative cost C on the model and ground truth MDP, because it may occur that model and ground truth diverge, but both give roughly the same cumulative cost C on average.

As indicated in (9), we assume that the true dynamics are determined by a neural network with latent variables and weights given by $\mathcal{W}_{\text{true}}$. By using the approximate posterior $q(\mathcal{W})$, and assuming that $\mathcal{W}_{\text{true}} \sim q(\mathcal{W})$, we can obtain an upper bound on the expected model bias as follows:

$$\begin{aligned} \mathbf{E}_{q(\mathcal{W})}[b(\mathcal{W}_\pi | \mathbf{s}_0)] &= \mathbf{E}_{\mathcal{W}_{\text{true}} \sim q(\mathcal{W})} \sum_{t=1}^T |\mathbf{E}[c_t | \mathcal{W}_{\text{true}}] - \mathbf{E}_{q(\mathcal{W})}[c_t]| \\ &\leq \sum_{t=1}^T \sqrt{\mathbf{E}_{\mathcal{W}_{\text{true}} \sim q(\mathcal{W})}(\mathbf{E}[c_t | \mathcal{W}_{\text{true}}] - \mathbf{E}_{q(\mathcal{W})}[c_t])^2} \\ &= \sum_{t=1}^T \sqrt{\sigma_{\mathcal{W}_{\text{true}} \sim q(\mathcal{W})}^2(\mathbf{E}[c_t | \mathcal{W}_{\text{true}}])} \\ &= \sum_{t=1}^T \sigma_{\mathcal{W}_{\text{true}} \sim q(\mathcal{W})}(\mathbf{E}[c_t | \mathcal{W}_{\text{true}}]). \end{aligned} \quad (14)$$

The last equation in (14) can be interpreted as the variability of the cost, that originates from our uncertainty over the dynamics given by distribution $q(\mathcal{W})$. We therefore will refer to $\sigma_{q(\mathcal{W})}(\mathbf{E}[c_t | \mathcal{W}])$ as the model bias risk criterion.

We extend the policy search objective of (10) with two risk components given by the model bias risk and the noise risk criterion. Similar to Depeweg et al. [2016], we derive a Monte Carlo approximation that enables optimization by gradient descent. Given a starting state \mathbf{s}_0 , we perform $M \times N$ roll-outs by first sampling $w \sim q(\mathcal{W})$ a total of M times and then, for each of these samples of $q(\mathcal{W})$, performing N roll-outs in which w is fixed and we only sample the latent variables z and the additive Gaussian noise. In particular,

$$\begin{aligned} J(\mathcal{W}_\pi | \mathbf{s}_0) &= \sum_{t=1}^T \left\{ \mathbf{E}[c_t] + \left(\beta^2 \sigma_{q(\mathcal{W})}^2(\mathbf{E}[c_t | \mathcal{W}]) + \gamma^2 \mathbf{E}_{q(\mathcal{W})}[\sigma^2(c_t | \mathcal{W})] \right)^{\frac{1}{2}} \right\} \\ &\approx \sum_{t=1}^T \left\{ \frac{1}{MN} \left[\sum_{m=1}^M \sum_{n=1}^N c_{m,n}(t) + \right. \right. \end{aligned}$$

$$\left. \left(\beta^2 \hat{\sigma}_M^2 \left(\frac{1}{N} \sum_{n=1}^N c_{m,n}(t) \right) + \gamma^2 \frac{1}{M} \sum_{m=1}^M \hat{\sigma}_N^2(c_{m,n}(t)) \right)^{\frac{1}{2}} \right\}, \quad (15)$$

where $c_{m,n}(t) = c(\mathbf{s}_t^{\mathcal{W}^m, \{z_1^{m,n}, \dots, z_t^{m,n}\}, \{\epsilon_1^{m,n}, \dots, \epsilon_t^{m,n}\}}, \mathcal{W}_\pi)$ is the cost that is obtained at time t in a roll-out generated by using a policy with parameters \mathcal{W}_π , a transition function parameterized by \mathcal{W}^m and latent variable values $z_1^{m,n}, \dots, z_t^{m,n}$, with additive noise values $\epsilon_1^{m,n}, \dots, \epsilon_t^{m,n}$. $\hat{\sigma}_M^2$ is an empirical estimate of the variance calculated over M draws of \mathcal{W} .

For $\gamma = 0$ the right hand side of Eq. (15) simplifies to $\beta \sigma_{q(\mathcal{W})}(\mathbf{E}[c_t | \mathcal{W}])$ which is the model bias risk given by Eq. (14). For $\beta = 0$ the right hand side simplifies to $\gamma \mathbf{E}_{q(\mathcal{W})}[\sigma^2(c_t | \mathcal{W})]^{\frac{1}{2}}$ which is the noise risk criterion. For $\beta = \gamma$ it simplifies to the standard deviation $\beta \sigma_{q(\mathcal{W})}(c_t)$. The goal of our approach is optimize policy quality as well as policy reliability (via the weighting parameter β). The second free parameter γ regulates the noise aversion. In real-world systems we often find a correlation between sub-optimal, possibly even dangerous, states and stochasticity. In specific settings, using $\gamma > 0$ can be useful to avoid those states.

5.1 Application: Industrial Benchmark

We show now the effectiveness of our proposed method the industrial benchmark, a stochastic system with properties inspired by real industrial systems [Hein et al., 2017].

Policies in the industrial benchmark specify changes Δ_v , Δ_g and Δ_s in three steering variables v (velocity), g (gain) and s (shift) as a function of \mathbf{s}_t . In the behavior policy these changes are stochastic and sampled according to

$$\Delta_v = \begin{cases} z_v, & \text{if } v(t) < 40 \\ -z_v, & \text{if } v(t) > 60 \\ u_v, & \text{otherwise} \end{cases} \quad (16)$$

$$\Delta_g = \begin{cases} z_g, & \text{if } g(t) < 40 \\ -z_g, & \text{if } g(t) > 60 \\ u_g, & \text{otherwise} \end{cases} \quad (17)$$

$$\Delta_s = u_s, \quad (18)$$

where $z_v, z_g \sim \mathcal{N}(0.5, \frac{1}{\sqrt{3}})$ and $u_v, u_g, u_s \sim \mathcal{U}(-1, 1)$. The velocity $v(t)$ and gain $g(t)$ can take values in $[0, 100]$. Therefore, the data collection policy will try to keep these values only in the medium range given by the interval $[40, 60]$. Because of this, large parts of the state space will be unobserved. After collecting the data, the 30,000 state transitions are used to train a BNN with latent variables with the same hyperparameters as in Depeweg et al. [2016]. Finally, we train different policies using the Monte Carlo approximation described in equation (15), we set the horizon of $T = 100$ steps, with $M = 50$ and $N = 25$ and a minibatch size of 1.

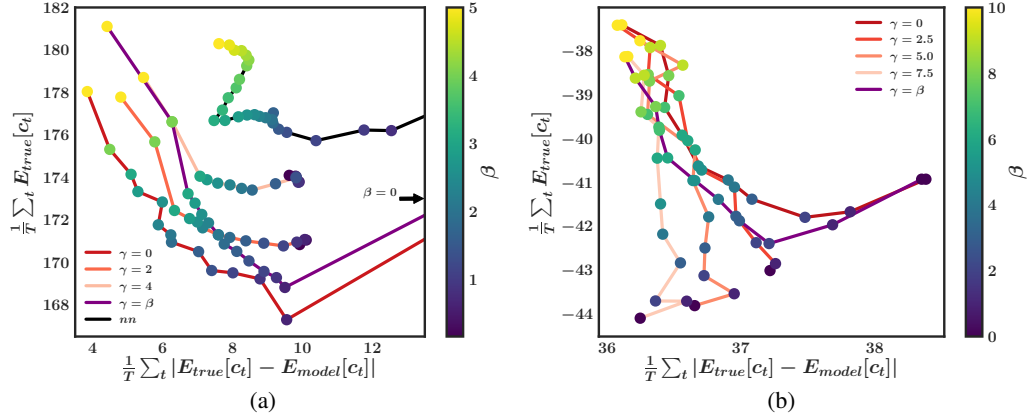


Figure 4: RL experiments: Fig. (a) shows results from experiments on the Industrial Benchmark. Fig. (b) shows results on the wind turbine simulator. Each curve shows the policy cost (y-axis) against the model bias (x-axis). Each individual curve is a function of different values of β (model bias weight), which is indicated by the color of circles. The color of the whole curve indicates different values of γ (noise risk weight), from dark red to bright red. The purple curve is the baseline $\beta\sigma(c_t)$, obtained by setting $\gamma = \beta$ in Eq. (15). The black curve is nearest neighbor baseline.

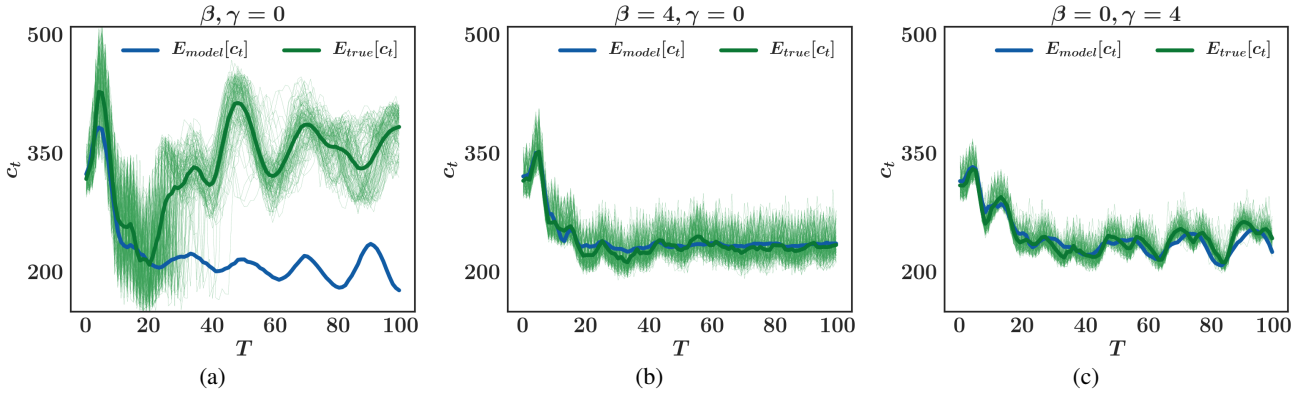


Figure 5: 100 roll-outs on ground truth (light green), their expectation (dark green), and their expectation on the model (blue) for 3 policies on the Industrial Benchmark for one start state s_0 . Policies have different model-bias risk weight β and noise risk weight γ (from Eq. (15)). Policies are optimized using (a): $\mathbf{E}[c_t]$ without model bias and noise risk ($\beta, \gamma = 0$). (b): $\mathbf{E}[c_t] + 4\sigma_{q(\mathcal{W})}(\mathbf{E}[c_t|\mathcal{W}])$ without noise risk ($\gamma = 0$). (c): $\mathbf{E}[c_t] + 4(\mathbf{E}_{q(\mathcal{W})}[\sigma^2(c_t|\mathcal{W})])^{\frac{1}{2}}$ without model bias risk ($\beta = 0$).

We measure performance using two different objectives: the expected cost obtained under the ground truth dynamics of the system, that is $\sum_{t=1}^T \mathbf{E}_{true}[c_t]$. The second objective is the model bias as defined in equation (13). We see how these objectives change for different choices of β and γ . This also gives us two baselines: when both β and γ are zero, the policy optimization ignores any risk and, therefore, is obtained by just optimizing equation (10). When $\beta = \gamma$ the optimization simplifies to $\beta\sigma(c_t)$, which is similar to the traditional risk-sensitive approach in Eq. (11). Lastly, our third baseline is using a standard neural network with a nearest neighbor approach as risk measure: for each state s_t generated in a roll-out we calculate the euclidean distance to the closest state in batch D and use this distance as risk metric, we denote this as the *nn*-baseline.

Figure 4a compares our method and the baselines to the ground truth. Each individual curve in this figure is a function over β . The policy that ignores any risk (first baseline) results in both high model bias and policy costs when evaluated on the ground truth, which indicates overfitting. As β increases the policies put more emphasis on avoiding model bias at the cost of slightly lower performance. The best tradeoff between policy cost and model bias is obtained by the dark red curve with $\gamma = 0$, the risk criterion is $\beta\sigma_{\mathcal{W} \sim q(\mathcal{W})}(\mathbf{E}[c_t|\mathcal{W}])$. Here, adding noise risk with $\gamma > 0$ decreases performance. The *nn* baseline shows a similar pattern, lowering model bias but increasing costs, but the trade-off is worse than in our proposed approach.

In Figure 5 we show roll-outs of 3 policies for the same starting state s_0 on the ground truth. In Fig. 5a the pol-

icy only minimizes expected cost during training. Starting around $T = 20$, the mismatch between the predicted performance on the model and the behavior on the ground truth increases—showing how model bias can lead to policies that produce high costs at evaluation. In Fig. 5b the policy optimizes expected cost and model bias risk. The behavior of the model and the ground truth are similar, and the ground truth cost is lower than in Fig. 5a. The policy in Fig. 5c is noise averse: it optimizes the expected cost and the noise risk. Compared to Fig. 5b we see a higher model bias, but significantly less stochasticity (smaller small green curves).

5.2 Application: Wind Turbine Simulation

We apply our method to a modified version of the HAWC2 wind turbine simulator [Larsen and Hansen, 2007], which is widely used for the study of wind turbine dynamics (see e.g., Larsen et al. [2015]); in this problem we observe the turbine state $s(t)$, with features such as current wind speed and currently produced power. Our actions $a(t)$ adjust the turbine’s behavior, with known upper and lower bounds. The goal is to maximize energy output over a T -step horizon.

We are given a batch of around 5,000 state transitions generated by a behavior policy π_b . The behavior policy is of similar structure as in the previous experiments, it tries to keep the system dynamics constrained to a manifold in state space. The system is expected to be highly stochastic due to the unpredictability of future wind dynamics. Furthermore the dimensionality of state observation is much higher than the action dimensionality, so, with the limited dataset that we have, we expect it to be very challenging to accurately learn the influence of the action on the reward.

First we train a BNN with two hidden layer and 50 hidden units per layer on the available batch using α -divergence minimisation with $\alpha = 1.0$. In the second step, using the model, we train a policy with 20 hidden units on each of the two layers in the usual way, using the Monte Carlo estimate of Eq. (15).

In Fig. 4b we show the results when evaluating the policies on the simulator. Each point in a curve indicates a different weighting of the model bias risk term β . As before, we see that small, but nonzero values of β reduce both policy costs as well as decrease model bias. A moderate regularization by β prevents the policy from overfitting the model too much. As β increases the model bias is reduced but costs increase. Each curve was generated using a different value of γ , e.g the desaturated red curve in Fig. 4b uses $\gamma = 7.5$ which means the policy will try to avoid noisy regions in state space. Unlike in the previous experiment, being noise averse is a good heuristic: the best result is obtained using $\gamma = 7.5$. This makes sense, because with wind turbines, high noise regions are those where the effect of wind (and in particular turbulence) will have a strong impact on performance.

6 Related Work

The distinction between aleatoric and epistemic uncertainty has been recognized in many fields within machine learning, often within the context of specific subfields, models, and objectives. Kendall and Gal [2017] consider a decomposition of uncertainty in the context of computer vision. However, rather than general stochastic models based on latent variables, they focus only on heteroskedastic, gaussian output noise. Perhaps most similar to our work is McAllister [2016]. In chapter 4.5, they discuss a similar decomposition using a Gaussian process model for exploration. The GP model, however, is not as scalable as our BNN approach and, in that work, the GP does not use latent variables.

Within reinforcement learning, Bayesian notions of model uncertainty have a long history [Schmidhuber, 1991b,a, Dearden et al., 1999, Still and Precup, 2012, Sun et al., 2011, Maddison et al., 2017, Mihatsch and Neuneier, 2002]. These works typically consider the online case, in which model uncertainty (a.k.a. curiosity) is used to guide exploration. For instance, in Houthoofd et al. [2016] the uncertainty of a BNN model is used to guide exploration assuming deterministic dynamics. In contrast, we focus on the batch setting with stochastic dynamics.

In the batch reinforcement learning setting, Joseph et al. [2013] address model (representational) bias by avoiding building a model all together; instead, they generate pseudo on-policy trajectories using model-free Monte Carlo, a form of local interpolation between real samples from the batch.

Model uncertainty is often used as part of a safe or risk-sensitive learning objective. For example, the work in Berkenkamp et al. [2017] and Garcia and Fernández [2012] approaches the problem of safe exploration, the former by using a Lyapunov stability verification and the latter by gradually improving over a predefined (and safe) baseline policy (For a comprehensive review of risk-sensitive RL we refer to Shen et al. [2014]). In contrast, we consider the question of *reliable* reinforcement learning in batch settings.

Within active learning, to our knowledge there is little work on learning stochastic functions. Our information-theoretic approach follows MacKay [1992], Hernández-Lobato and Adams [2015], which assume deterministic dynamics.

7 Conclusion

We have studied a decomposition of predictive uncertainty into its epistemic and aleatoric components when working with Bayesian neural networks with latent variables. This decomposition naturally arises when applying information-theoretic active learning setting, and it also enabled us to derive a novel risk objective for reliable reinforcement learning by decomposing risk into a model bias and noise. In both of these settings, our approach allows us to efficiently learn in the face of sophisticated stochastic functions.

References

- F. Berkenkamp, M. Turchetta, A. P. Schoellig, and A. Krause. Safe model-based reinforcement learning with stability guarantees. *arXiv preprint arXiv:1705.08551*, 2017.
- C. Blundell, J. Cornebise, K. Kavukcuoglu, and D. Wierstra. Weight uncertainty in neural networks. *arXiv preprint arXiv:1505.05424*, 2015.
- R. Dearden, N. Friedman, and D. Andre. Model based bayesian exploration. In *Proceedings of the Fifteenth conference on Uncertainty in artificial intelligence*, pages 150–159. Morgan Kaufmann Publishers Inc., 1999.
- M. P. Deisenroth, G. Neumann, J. Peters, et al. A survey on policy search for robotics. *Foundations and Trends® in Robotics*, 2(1–2):1–142, 2013.
- S. Depeweg, J. M. Hernández-Lobato, F. Doshi-Velez, and S. Udluft. Learning and policy search in stochastic dynamical systems with bayesian neural networks. *arXiv preprint arXiv:1605.07127*, 2016.
- Y. Gal, R. T. McAllister, and C. E. Rasmussen. Improving pilco with bayesian neural network dynamics models. In *Data-Efficient Machine Learning workshop*, volume 951, page 2016, 2016.
- W. Gao, S. Oh, and P. Viswanath. Breaking the bandwidth barrier: Geometrical adaptive entropy estimation. In *Advances in Neural Information Processing Systems*, pages 2460–2468, 2016.
- J. Garcia and F. Fernández. Safe exploration of state and action spaces in reinforcement learning. *Journal of Artificial Intelligence Research*, 45:515–564, 2012.
- J. García and F. Fernández. A comprehensive survey on safe reinforcement learning. *The Journal of Machine Learning Research*, 16(1):1437–1480, 2015.
- A. Hans and S. Udluft. Efficient uncertainty propagation for reinforcement learning with limited data. In *ICANN*, pages 70–79. Springer, 2009.
- D. Hein, S. Depeweg, M. Tokic, S. Udluft, A. Hentschel, T. A. Runzler, and V. Sterzing. A benchmark environment motivated by industrial control problems. *arXiv preprint arXiv:1709.09480*, 2017.
- J. M. Hernández-Lobato and R. P. Adams. Probabilistic backpropagation for scalable learning of bayesian neural networks. *arXiv preprint arXiv:1502.05336*, 2015.
- J. M. Hernández-Lobato, Y. Li, M. Rowland, D. Hernández-Lobato, T. Bui, and R. E. Turner. Black-box α -divergence minimization. In *Proceedings of The 33rd International Conference on Machine Learning (ICML)*, 2016.
- R. Houthoofd, X. Chen, Y. Duan, J. Schulman, F. De Turck, and P. Abbeel. VIME: Variational information maximizing exploration. In *Advances in Neural Information Processing Systems*, pages 1109–1117, 2016.
- J. Joseph, A. Geramifard, J. W. Roberts, J. P. How, and N. Roy. Reinforcement learning with misspecified model classes. In *Robotics and Automation (ICRA), 2013 IEEE International Conference on*, pages 939–946. IEEE, 2013.
- A. Kendall and Y. Gal. What uncertainties do we need in bayesian deep learning for computer vision? *arXiv preprint arXiv:1703.04977*, 2017.
- A. D. Kiureghian and O. Ditlevsen. Aleatory or epistemic? does it matter? *Structural Safety*, 31(2):105 – 112, 2009. Risk Acceptance and Risk Communication.
- L. Kozachenko and N. N. Leonenko. Sample estimate of the entropy of a random vector. *Problemy Peredachi Informatsii*, 23(2):9–16, 1987.
- A. Kraskov, H. Stögbauer, and P. Grassberger. Estimating mutual information. *Physical review E*, 69(6):066138, 2004.
- T. J. Larsen and A. M. Hansen. How 2 hawc2, the user’s manual. Technical report, Risø National Laboratory, 2007.
- T. J. Larsen, G. Larsen, H. A. Madsen, K. Thomsen, and S. M. Pedersen. Comparison of measured and simulated loads for the siemens swt2.3 operating in wake conditions at the lillgrund wind farm using hawc2 and the dynamic wake meander model. *EWEA offshore 2015*, 2015.
- D. J. MacKay. Information-based objective functions for active data selection. *Neural computation*, 4(4):590–604, 1992.
- C. J. Maddison, D. Lawson, G. Tucker, N. Heess, A. Doucet, A. Mnih, and Y. W. Teh. Particle value functions. *arXiv preprint arXiv:1703.05820*, 2017.
- R. McAllister. *Bayesian Learning for Data-Efficient Control*. PhD thesis, Kings College, 2016.
- O. Mihatsch and R. Neuneier. Risk-sensitive reinforcement learning. *Machine learning*, 49(2-3):267–290, 2002.
- T. M. Moerland, J. Broekens, and C. M. Jonker. Learning multimodal transition dynamics for model-based reinforcement learning. *arXiv preprint arXiv:1705.00470*, 2017.
- J. Schmidhuber. Curious model-building control systems. In *Neural Networks, 1991. 1991 IEEE International Joint Conference on*, pages 1458–1463. IEEE, 1991a.
- J. Schmidhuber. A possibility for implementing curiosity and boredom in model-building neural controllers. In *From animals to animats: Proceedings of the first international conference on simulation of adaptive behavior*, pages 15–21. Citeseer, 1991b.
- D. Schneegass, S. Udluft, and T. Martinetz. Uncertainty propagation for quality assurance in reinforcement learning. In *Neural Networks, 2008. IJCNN 2008. (IEEE World Congress on Computational Intelligence). IEEE International Joint Conference on*, pages 2588–2595. IEEE, 2008.
- Y. Shen, M. J. Tobia, T. Sommer, and K. Obermayer. Risk-sensitive reinforcement learning. *Neural computation*, 26(7):1298–1328, 2014.
- S. Still and D. Precup. An information-theoretic approach to curiosity-driven reinforcement learning. *Theory in Biosciences*, 131(3):139–148, 2012.
- Y. Sun, F. Gomez, and J. Schmidhuber. Planning to be surprised: Optimal bayesian exploration in dynamic environments. In *International Conference on Artificial General Intelligence*, pages 41–51. Springer, 2011.

A Hamiltonian Monte Carlo Solution to Toy Problems

The goal here is to show that the decomposition we obtained in the active learning examples are not a result of our approximation using blackbox- α but a property of BNNs themselves. To that end we will approximate using HMC. After a burnin of 500,000 samples we sample from the posterior 200,000 samples. We thin out 90% by only keeping every tenth sample.

A.1 Heteroskedastic Problem

We define the stochastic function $y = 7 \sin(x) + 3|\cos(x/2)|\epsilon$ with $\epsilon \sim \mathcal{N}(0, 1)$. The data availability is limited to specific regions of x . In particular, we sample 750 values of x from a mixture of three Gaussians with mean parameters $\{\mu_1 = -4, \mu_2 = 0, \mu_3 = 4\}$, variance parameters $\{\sigma_1 = \frac{2}{5}, \sigma_2 = 0.9, \sigma_3 = \frac{2}{5}\}$ and with each Gaussian component having weight equal to $1/3$ in the mixture. Figure 6a shows the raw data. We have lots of points at both borders of the x axis and in the center, but little data available in between.

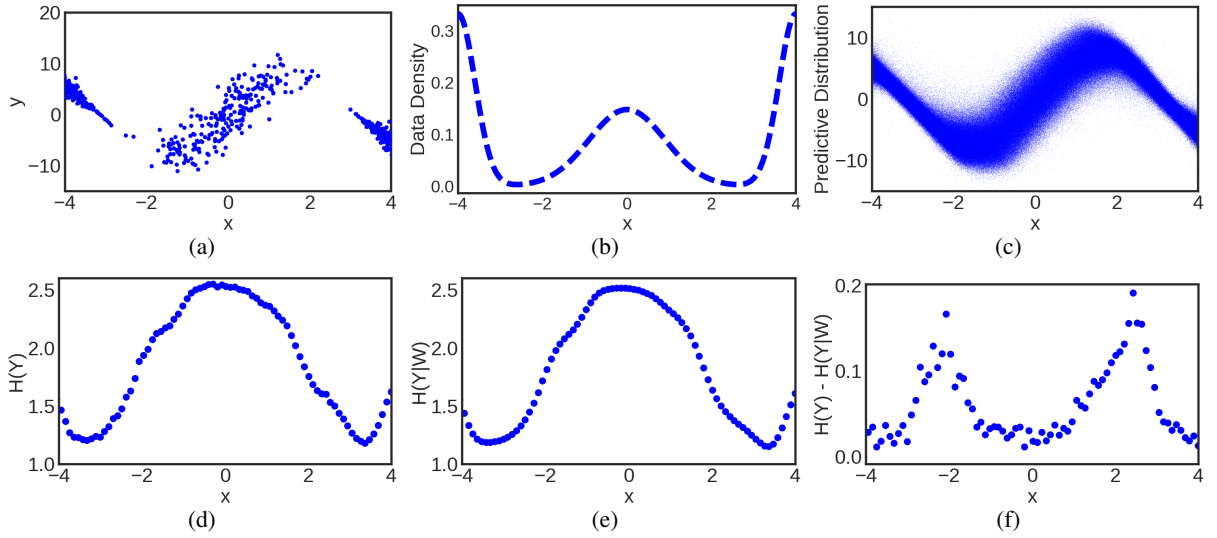


Figure 6: HMC results of active learning example using heteroskedastic data. (a): Raw data. (b): Density of x in raw data. (c): Predictive distribution: $p(y|x)$ of BNN using HMC. (d): Entropy estimate $H(y|x)$ of predictive distribution for each x . (e): Conditional Entropy estimate $E_{\mathcal{W}} H(y|x, \mathcal{W})$ of predictive distribution for each x . (f): Estimate of reduction in entropy for each x .

A.2 Bimodal Problem

We consider a toy problem given by a regression task with bimodal data. We define $x \in [-0.5, 2]$ and $y = 10 \sin(x) + \epsilon$ with probability 0.5 and $y = 10 \cos(x) + \epsilon$, otherwise, where $\epsilon \sim \mathcal{N}(0, 1)$ and ϵ is independent of x . The data availability is not uniform in x . In particular we sample 750 values of x from an exponential distribution with $\lambda = 2$

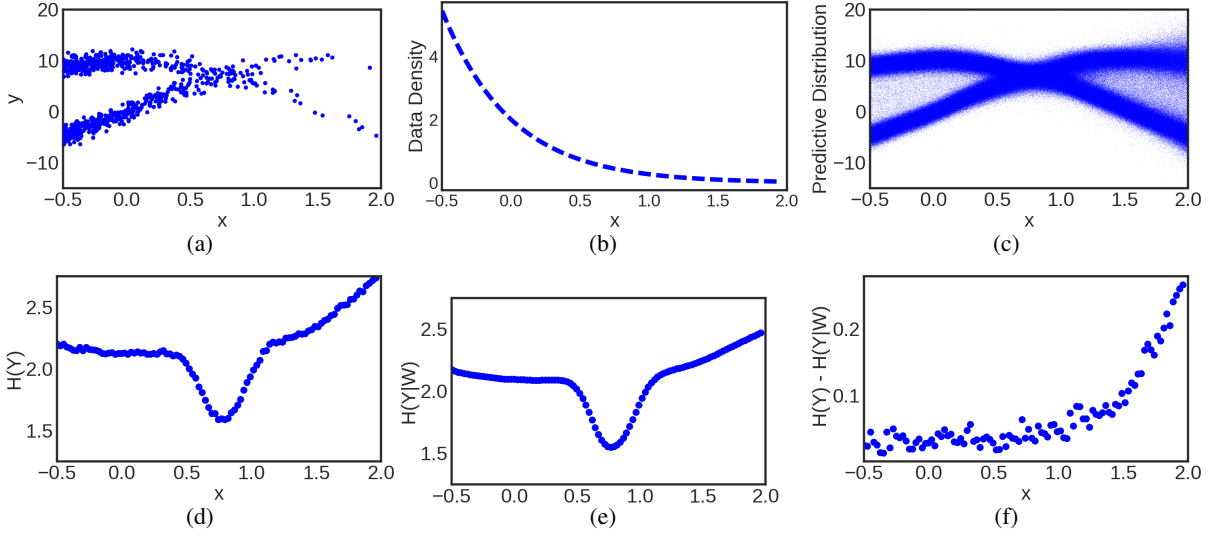


Figure 7: HMC results of active learning example using bimodal data. (a): Raw data. (b): Density of x in raw data. (c): Predictive distribution: $p(y|x)$ of BNN using Hamilton monte carlo. (d): Entropy estimate $H(y|x)$ of predictive distribution for each x . (e): Conditional Entropy estimate $\mathbb{E}_{\mathcal{W}}H(y|x, \mathcal{W})$ of predictive distribution for each x . (f): Estimate of reduction in entropy for each x .

B Solutions to Toy Problems for different values of α

In the main document we pointed out that the decomposition of uncertainty does not work as good with other values of α . We will see in the following, that lower values of α will put more and more emphasis on the latent variable z . We observe that the epistemic uncertainty will vanish as the α -divergence minimization approaches variational Bayes.

B.1 $\alpha = 0.5$

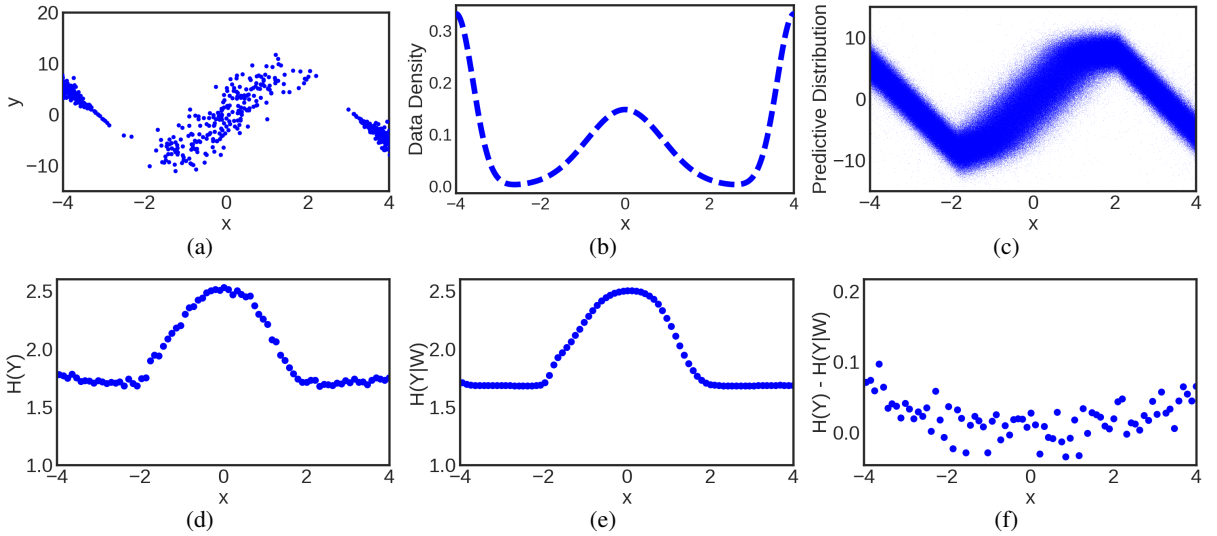


Figure 8: Active learning example using heteroskedastic data using a BNN optimized with $\text{bb-}\alpha$ with $\alpha = 0.5$. (a): Raw data. (b): Density of x in raw data. (c): Predictive distribution: $p(y|x)$ of BNN. (d): Entropy estimate $H(y|x)$ of predictive distribution for each x . (e): Conditional Entropy estimate $\mathbb{E}_{\mathcal{W}}H(y|x, \mathcal{W})$ of predictive distribution for each x . (f): Estimate of reduction in entropy for each x .

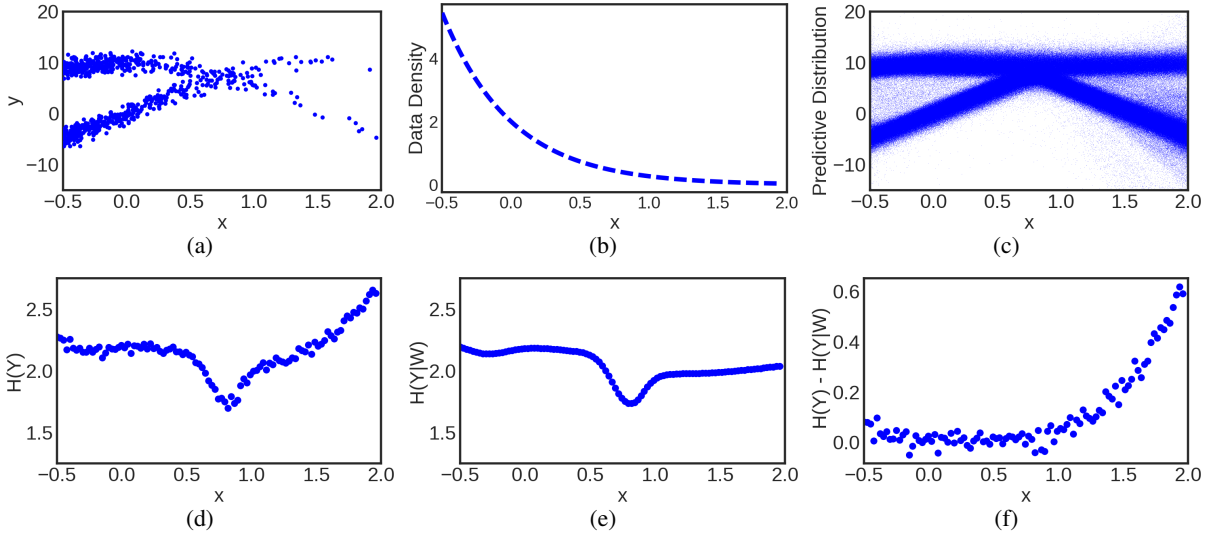


Figure 9: Active learning example using bimodal data using a BNN optimized with $\text{bb-}\alpha$ with $\alpha = 0.5$. (a): Raw data. (b): Density of x in raw data. (c): Predictive distribution: $p(y|x)$ of BNN. (d): Entropy estimate $H(y|x)$ of predictive distribution for each x . (e): Conditional Entropy estimate $\mathbb{E}_{\mathcal{W}} H(y|x, \mathcal{W})$ of predictive distribution for each x . (f): Estimate of reduction in entropy for each x .

B.2 VB solutions to Toy Problems

We approximate the method variational Bayes by setting α to 10^{-6} .

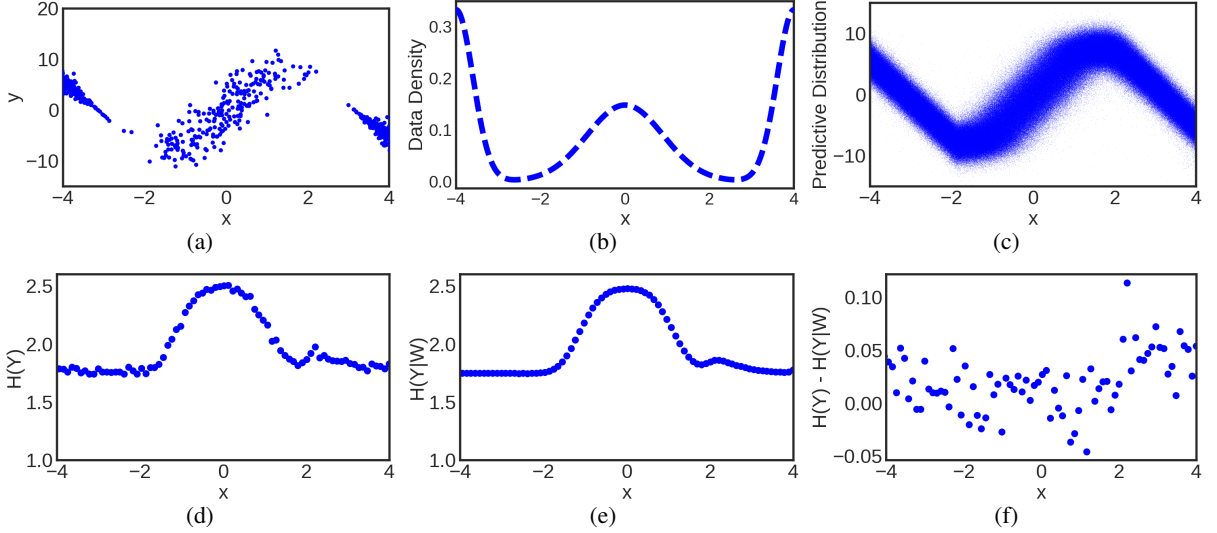


Figure 10: Active learning example using heteroskedastic data using a BNN optimized by variational Bayes. (a): Raw data. (b): Density of x in raw data. (c): Predictive distribution: $p(y|x)$ of BNN. (d): Entropy estimate $H(y|x)$ of predictive distribution for each x . (e): Conditional Entropy estimate $\mathbb{E}_{\mathcal{W}} H(y|x, \mathcal{W})$ of predictive distribution for each x . (f): Estimate of reduction in entropy for each x .

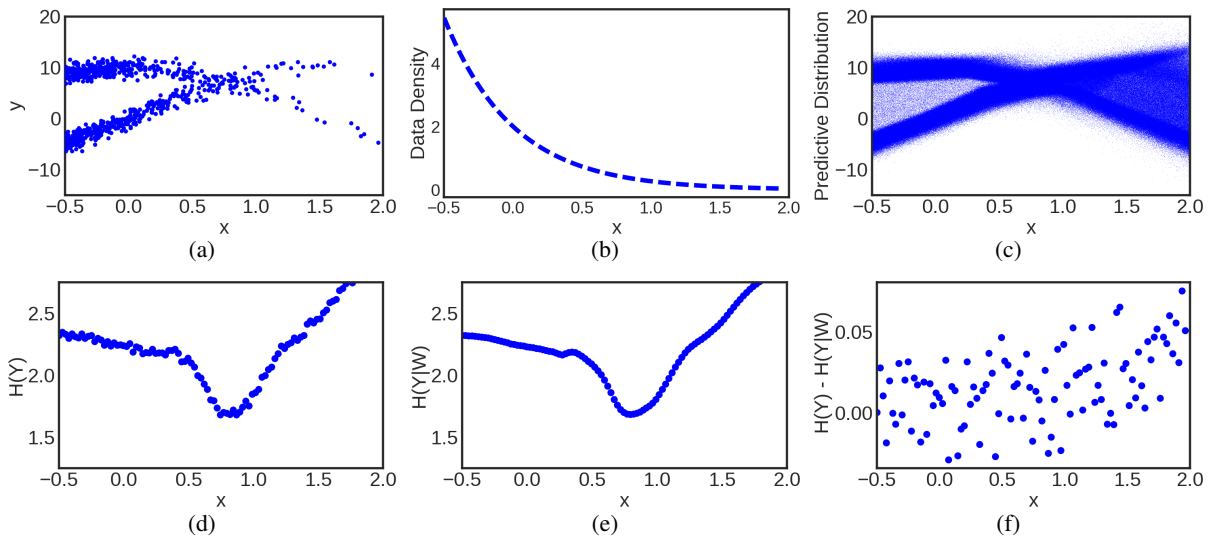


Figure 11: Active learning example using bimodal data using a BNN optimized by variational Bayes. (a): Raw data. (b): Density of x in raw data. (c): Predictive distribution: $p(y|x)$ of BNN. (d): Entropy estimate $H(y|x)$ of predictive distribution for each x . (e): Conditional Entropy estimate $\mathbb{E}_{\mathcal{W}} H(y|x, \mathcal{W})$ of predictive distribution for each x . (f): Estimate of reduction in entropy for each x .